



Title	柔軟エアロシェルを有する大気突入機の流体構造連成解析
Author(s)	サハ, サンジョイ クマー; 高橋, 裕介
Citation	サイバーメディアHPCジャーナル. 2024, 14, p. 113-119
Version Type	VoR
URL	https://doi.org/10.18910/96538
rights	
Note	

The University of Osaka Institutional Knowledge Archive : OUKA

<https://ir.library.osaka-u.ac.jp/>

The University of Osaka

柔軟エアロシェルを有する大気突入機の流体構造連成解析

Fluid-structure interaction analysis for atmospheric-entry vehicle with inflatable aeroshell

サンジョイ・クマー・サハ、高橋裕介

北海道大学 大学院工学研究院

SAHA Sanjoy Kumar and TAKAHASHI Yusuke

Faculty of Engineering, Hokkaido University, Japan

1. Introduction

In recent years, there has been considerable research attention on inflatable aeroshell technology, which offers distinct advantages compared to traditional rigid heat shields. In Japan, the development of an inflatable aeroshell system known as the Membrane Aeroshell for Atmospheric-Entry Capsule (MAAC) has been a focal point [1-2]. This innovative aeroshell comprises a rigid capsule, a thin, flexible membrane, and an inflatable torus pressurized with gas to maintain its shape, as depicted in Fig. 1. The Japan Aerospace Exploration Agency (JAXA) has undertaken numerous flight experiments employing scientific balloons and rockets to assess the viability of utilizing a membrane aeroshell for deceleration purposes. A flight test conducted in 2012 revealed challenges associated with operating the aeroshell at low Mach numbers, where instability in attitude and significant aerodynamic forces, coupled with fluctuations in inflation pressure, were identified as potential factors contributing to aeroshell collapse [3].

The deformation of the membrane surface under the peak freestream dynamic pressure resulted in a change in the flare angle, which could not regain its original shape thereafter. Furthermore, the drag coefficient profile observed during flight tests differed from that obtained in wind tunnel experiments [4]. The flexible nature of the membrane makes it susceptible to deformation, leading to potential instabilities and increased thermal loads due to turbulence effects. At transonic speeds, aerodynamic stresses on the aeroshell are very intense, resulting in frequent structural failures owing to aeroelastic interactions [5]. However, a thorough understanding of the underlying processes causing such failures remains inadequate. To effectively forecast the behavior of reentry vehicles, coupled studies must be conducted that account for the feedback impact of structural deformation. Coupled analyses, by definition, entail unsteady behavior, such as limit-cycle oscillations, which make understanding difficult. Dynamic Mode Decomposition (DMD) is among the reduced-order models that decompose large-scale spatiotemporal data into distinct spatial and temporal modes, extracting patterns with characteristic frequencies. Keeping this background in mind, this study aims to elucidate the deformation behavior of the deployable aeroshell using a coupled model and to unveil its spatial patterns and temporal behavior through modal decomposition under the transonic flow regime.

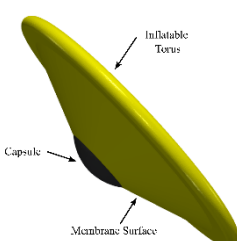


Fig. 1: Flare type inflatable membrane aeroshell

2. Numerical Methods

2.1 Coupled Analysis Model

The aerodynamic behavior of the aeroshell in transonic fluid flow is described by the three-dimensional compressible Navier-Stokes equation and the equation of state. To solve these equations, we employ a vertex-centered finite volume method implemented in the open-source unstructured mesh fluid flow solver SU2 [6]. To approximate the viscous terms, the mean of flow property gradients across adjacent cells is computed, utilizing the Green-Gauss approach to obtain spatial gradients. The viscosity coefficient is determined using Sutherland's formula. The Jameson-Schmidt-Turkel (JST) method [7] is employed as the advection scheme with second-order dual time-stepping. Matrix solutions are obtained using the FGMRES method, and the research excludes turbulence models. Domain decomposition and MPI are utilized for parallel computation of the extensive problem.

The governing equation of structural dynamics is based on the principle of virtual work and discretized with respect to microelements. It consists of the displacement field within each element, an element stiffness matrix, an element load vector, and an element mass matrix. The load vector, stiffness matrix, and mass matrix are computed for each element. The α -method is employed with Gauss-Legendre quadrature integration to solve the overall stiffness equation. However, the current approach does not account for the nonlinearity of material characteristics. CalculiX [8] is used to examine the nonlinear dynamics of a membrane aeroshell coupled with the help of an adapter. The nonlinear structural behavior under dynamic stress is evaluated using implicit integration of equations of motion, considering it as a three-dimensional continuum with constant temperature during analysis.

The partitioned coupling strategy is selected for this application. preCICE [9] is utilized as a coupling

library to couple the flow solver SU2 to the structural solver CalculiX. During analysis, an adapter is included for each solver. The coupling process assumes that the continuity and equilibrium conditions are consistently fulfilled on the coupled interface. The fluid solver transmits the aerodynamic forces to the coupled interface while receiving displacement information from the structural solver. The nearest-neighbor data mapping algorithms is incorporated to facilitate the data exchange between non-matching grids. TCP/IP sockets have been used to allow for efficient data flow between the solvers. To meet the continuity and equilibrium conditions, the parallel-implicit coupling technique is adopted with the Interface Quasi-Newton convergence acceleration scheme in the iterations. Adopting these schemes increased the computational cost significantly. However, the stability of the coupling process increased.

2.2 Dynamic Mode Decomposition

The data-driven technique namely DMD, originally invented by Schmid [10], is used to extract coherent patterns and dynamic behavior from complex, high-dimensional datasets, offering insights into underlying system dynamics, modes, and frequencies. Utilizing a time-series matrix \mathbf{D} comprised of flow field data matrices \mathbf{u} captured at distinct spatial points and time instances, shown as Eq. (1), it is possible to capture the temporal evolution of the entire system through the application of a time transition matrix \mathbf{A} .

$$\mathbf{D} = [\mathbf{u}_0, \mathbf{u}_1, \dots, \mathbf{u}_{n+1}] \quad (1)$$

$$\begin{aligned} \mathbf{X} &= [\mathbf{u}_0, \mathbf{u}_1, \dots, \mathbf{u}_n], \quad \mathbf{Y} = [\mathbf{u}_1, \mathbf{u}_2, \dots, \mathbf{u}_{n+1}] \\ \mathbf{Y} &= \mathbf{AX} \end{aligned} \quad (2)$$

$$\mathbf{A}\Phi = \Phi\Lambda \Rightarrow \mathbf{A} = \Phi\Lambda\Phi^\dagger \quad (3)$$

$$\mathbf{Y} = \mathbf{AX} = \Phi\Lambda\Phi^\dagger\mathbf{X} \quad (4)$$

$$\mathbf{u}(t) = \Phi\Lambda^{t/\Delta t}\Phi^\dagger\mathbf{u}(0) \quad (5)$$

Two matrix \mathbf{X} and \mathbf{Y} can be defined by Eq. (2).

From the result of the singular value decomposition of \mathbf{X} , we can obtain the result of the eigenvalue decomposition of \mathbf{A} . Using the eigenvalue matrix Λ , eigenvector matrix ϕ and coefficient matrix vector Φ^\dagger , we can reconstruct $u(t)$. Due to the increasing computational intricacy associated with eigenvalue decomposition for sizable \mathbf{A} matrices, we implement the Exact Dynamic Mode Decomposition (Exact DMD) [11] method. We decompose matrix \mathbf{X} into singular values, selectively employing pertinent modes. Subsequently, matrix \mathbf{A} is projected, followed by eigenvalue decomposition. The eigenvector matrix ϕ represents the dynamic modes, each contributing uniquely to the system, while the eigenvalue matrix Λ , a complex structure, characterizes system changes (magnitude and amplitude).

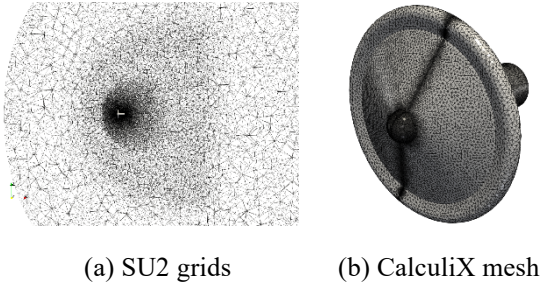


Fig. 2: Grids for fluid and structural analysis

3. Analysis Conditions

The numerical analyses are conducted on a scaled model of the membrane aeroshell, constructed with high-strength Zylon fabric for both the membrane surface and inflatable torus. The model dimensions include a diameter of 80 mm for the aeroshell, a membrane thickness of 0.15 mm, and a flare angle of 70°. The diameter of the inflatable torus is 6 mm, and for simplification purposes, the actual inflation mechanism is omitted from this study. The aeroshell is subjected to a uniform flow environment. This study selected specific Mach number of 0.9 while maintaining a constant angle of attack of 0° and a uniform flow dynamic pressure of 7.95, 4.49 and 0.19 kPa. The free stream Reynolds number is on the order

of 10^5 . The membrane surface is assumed to be fixed at a temperature of 300 K, with a no-slip condition and no pressure gradient in the normal direction. The computational domain for the fluid flow analysis consisted of 5,231,960 unstructured tetrahedral nodes, as illustrated in Fig. 2(a). A separate computational mesh having triangular shell elements is used for the structural simulation, as shown in Fig. 2(b). The capsule and the rear sting are treated as fixed boundaries, while the rest are designated as free boundaries and coupled interfaces. As the mechanical properties of Zylon, Young's modulus was set as 70 MPa, Poisson's ratio of 0.3, and density of 900 kg/m³.

4. Results

4.1 Aerodynamics and Elastic Deformation

The instantaneous distributions of the Mach number are shown in Fig. 3.

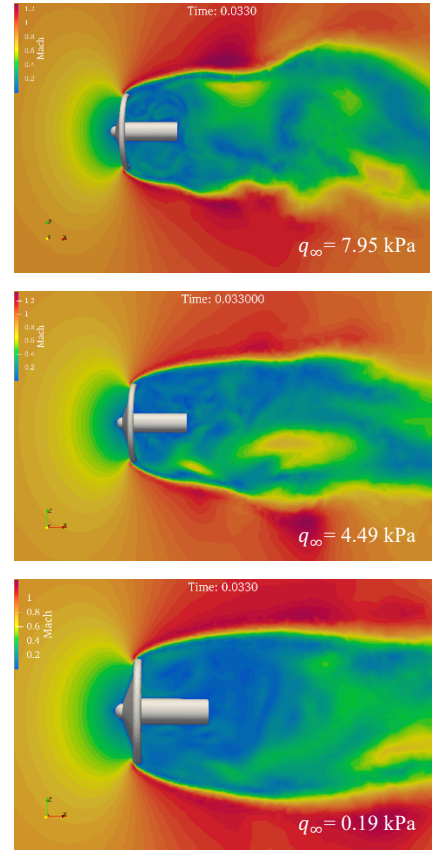
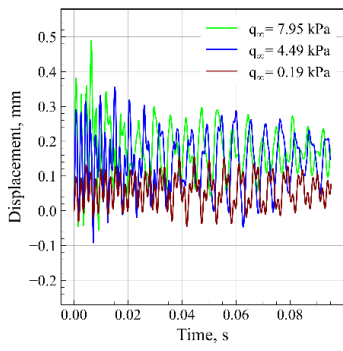


Fig. 3: Mach distributions for different cases

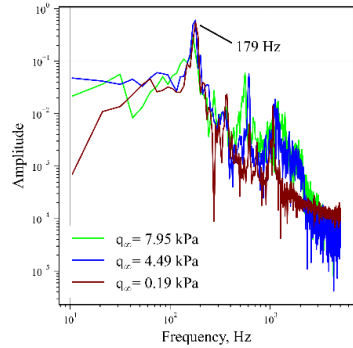
No shock wave appeared in any of the cases. The incoming high-speed flow stagnated in front of the

capsule, so a high-pressure region appeared in front, and a low-pressure region was formed at the rear side of the aeroshell. Flow separation occurred near the torus, accompanied by the expansion waves. In the large recirculation region formed behind the aeroshell, alternating vortices and thin shear layers were formed. The continuous generation and shedding of the wake vortex induced oscillation of the aeroshell.

The substantial membrane surface area of the inflatable aeroshell leads to flow stagnation, causing a pressure disparity between its front and rear regions. An adverse pressure gradient prompts flow separation from the inflatable torus, triggering the formation of vortex pairs. This dynamic process of wake vortex generation and shedding induces unsteady aerodynamics, manifesting as fluctuations and oscillations in the behavior of the aeroshell. Employing the probe technique, we tracked the positional variations of the inflatable torus across distinct positions. For evaluating displacement data along the three axes, two probe points were



(a) Torus displacement



(b) FFT of torus displacement

Fig. 4: Displacement and frequency plots

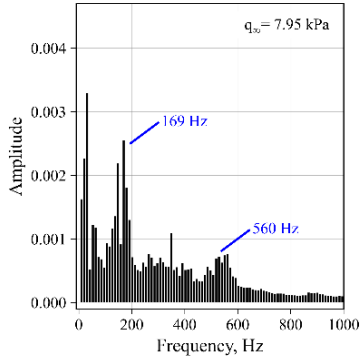
strategically positioned within the structural mesh, encompassing the upper and lower portions of the aeroshell. Figure 4 illustrates the instantaneous time-series data reflecting the torus displacement in flow directions and their frequency plots for all cases.

It is self-explanatory from Fig. 4(a) that the oscillation amplitude increases with higher dynamic pressure of the freestream. To obtain the frequency of such oscillation, Fast Fourier Transform (FFT) has been applied to the displacement data in x direction. From the frequency domain plot of the torus displacement, as shown in Fig. 4(b), it is evident that the peak frequency of oscillation is 179 Hz for each dynamic pressure cases even though the amplitudes are different.

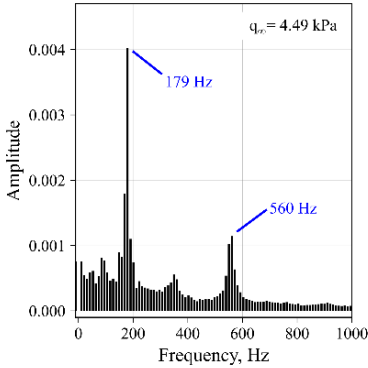
4.2 Dynamic Mode Decomposition

The dynamic mode decomposition approach is used on the structural displacement data obtained from the coupled analysis. The frequency distributions and corresponding amplitudes of the DMD modes are shown in Fig. 5. Several closely spaced modes with various frequencies up to 1000 Hz exist in the displacement spatiotemporal data. Notably, the high and mid-range dynamic pressure case exhibits peak frequencies around the same as obtained from the frequency plot of torus displacement (179 Hz). However, the low dynamic pressure case shows multitude of closely spaced frequencies, indicating a higher degree of oscillation and higher frequency than the other cases. To identify the physically important modes from the DMD modes with low computational cost, a greedy approach for compressive sensing has been adopted for this work [12]. Based on the greedy algorithm, two distinct frequency groups are identified for the primary and secondary modes.

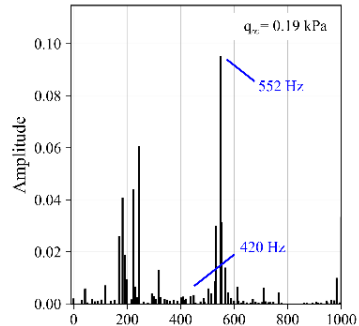
For the high and mid-range dynamic pressure cases, the primary mode group exhibits a frequency of 169 - 179 Hz, while the secondary mode group exhibits a frequency of 560 Hz. These two frequencies closely



(a) $q_{\infty} = 7.95 \text{ kPa}$



(b) $q_{\infty} = 4.49 \text{ kPa}$



(c) $q_{\infty} = 0.19 \text{ kPa}$

Fig. 5: Amplitude and frequency for DMD modes

correspond to the frequency obtained by the FFT method. In contrast, for the low dynamic pressure case, the primary mode group frequency is 552 Hz, and the secondary mode group frequency is 420 Hz.

The primary mode of the displacement for high and mid-range dynamic pressure cases are the membrane deformation, and the secondary mode is the oscillatory swinging motion, as shown in Fig. 6 and 7. On the other hand, for low dynamic pressure case, pitching oscillations are the dominant primary and secondary modes rather than membrane deformation, as shown in

Fig. 8. The contribution of each DMD modes to the aerodynamics and the combined oscillation is still under investigation at this point.

For the high and mid-range dynamic pressure cases, time evolution of the primary and secondary modes indicates that the DMD modes are purely oscillatory rather than exhibiting neither growth nor decay characteristics, shown in Fig. 9(a) and (b). However, the low dynamic pressure case exhibits increasing amplitude tendency with time. This observation indicates the inherent unsteady oscillatory behavior of the analyzed transonic dynamic pressure cases, shown in Fig. 9(c).

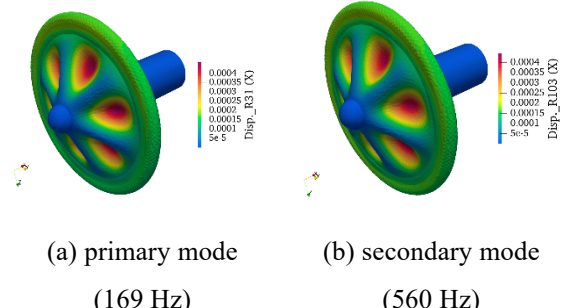


Fig. 6: Dominant mode groups for $q_{\infty} = 7.95 \text{ kPa}$

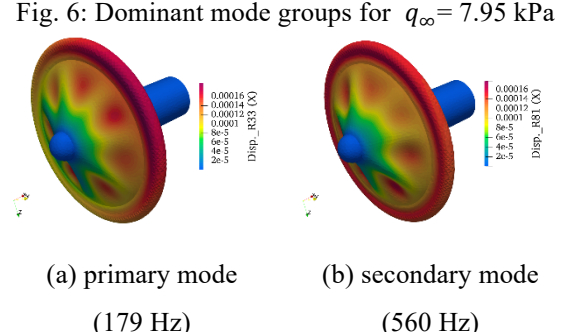


Fig. 7: Dominant mode groups for $q_{\infty} = 4.49 \text{ kPa}$

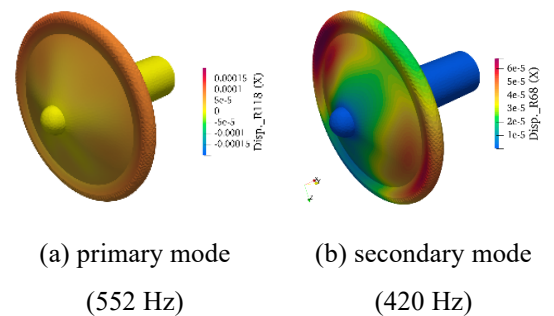
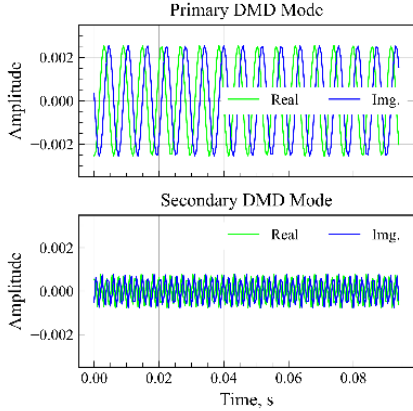
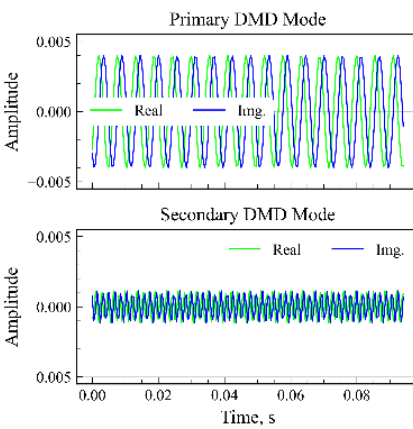


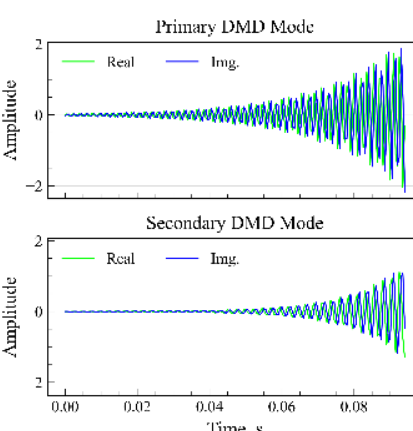
Fig. 8: Dominant mode groups for $q_{\infty} = 0.19 \text{ kPa}$



(a) $q_{\infty} = 7.95 \text{ kPa}$



(b) $q_{\infty} = 4.49 \text{ kPa}$



(c) $q_{\infty} = 0.19 \text{ kPa}$

Fig. 9: Evolution of dominant modes for different dynamic pressure cases

5. Conclusions

This research explored the unsteady fluid-structure

interaction behavior of a deployable aeroshell in

transonic flow, considering variations in freestream dynamic pressure. Additionally, dynamic mode decomposition (DMD) is employed to analyze coherent patterns within the system. Using the greedy compressive sensing algorithm, the dominant membrane deformation structures are identified. The results revealed that the dominant pattern of deformation is the combination of axial deformation and swing oscillation. The frequency of oscillation of the aeroshell is almost independent of the dynamic pressure. However, the amplitude of such oscillation is higher in the case of increasing dynamic pressure. The time evolution revealed that these dominant modes are purely oscillating with time rather than increasing or decreasing characteristics except the low dynamic pressure case. This study offered valuable insights into the complicated oscillation behavior of the deployable membrane aeroshell by decomposing structural deformation, enhancing the understanding of the complex dynamics involved in reentry processes.

Acknowledgement

This work was achieved through the use of SQUID at the Cybermedia Center, Osaka University.

References

- (1) Yamada, Kazuhiko, et al. 21st AIAA aerodynamic decelerator systems technology conference, (2011).
- (2) Yamada, Kazuhiko. 28th ISTS, Okinawa, (2011).
- (3) Takahashi, Yusuke, et al., Aerospace Science and Technology, **92** (2019): 858-868.
- (4) Yamada, Kazuhiko, et al. Journal of Spacecraft and Rockets 52.1 (2015): 275-284.
- (5) Saha, et al., AIAA SCITECH 2023 Forum. (2023).
- (6) Economou, Thomas D., et al. AIAA Journal 54.3 (2016): 828-846.
- (7) Jameson, Antony et al., AIAA Journal 55.5

(2017): 1487-1510.

- (8) Dhondt, G., & Wittig, K. (1998). A free software three-dimensional structural finite element program.
- (9) Bungartz, Hans-Joachim, et al., Computers & Fluids 141 (2016): 250-258.
- (10) Schmid, Peter J., Journal of fluid mechanics 656 (2010): 5-28.
- (11) Tu, Jonathan H. Dynamic mode decomposition: Theory and applications. Diss. Princeton University, 2013.
- (12) Ohmichi, Yuya., et al., AIP Advances 7.7 (2017).